4 Electronic Spectroscopy of the Au-Kr complex

4.1 Introduction

The Au-Kr complex was the second Au-RG complex to be studied at Nottingham. No previous work had been published in the open literature on this complex; however, spectra and the resulting analysis was found to be reported in a thesis chapter by Franz Wallimann.[1] This work reported spectra of the molecular states recorded in the vicinity of the Au $^2P_J \leftarrow {}^2S$ atomic transitions. Of the three molecular states in this energetic region, the $D^2\Pi_{1/2}$ state originating from the Au($^2P_{1/2}$) + Kr($^1S_0$) asymptote and the $D^2\Pi_{3/2}$ and $E^2\Sigma_{1/2}^+$ states both originating from the Au($^2P_{3/2}$) + Kr($^1S_0$) asymptote, only the two spin-orbit split $^2\Pi$ states were observed.

There are six naturally occurring isotopes[2] of Kr: ^{78}Kr (0.35%), ^{80}Kr (2.28%), ^{82}Kr (11.58%), ^{83}Kr (11.49%), ^{84}Kr (57.00%) and ^{86}Kr (17.30%) and one isotope of ^{197}Au, and therefore six possible isotopomers of Au-Kr. Wallimann reported spectra for five of these isotopomers for each observed state, from which, through the use of an isotopic analysis, he was able to determine the absolute vibrational numbering of the progression. Utilising the vibrational numbering, Wallimann fitted the vibrational levels to a Morse potential to derive a number of spectroscopic constants for the excited states. These parameters, in addition to the associated atomic transition and weakly observed hot bands, allowed spectroscopic constants of the ground state to be

estimated. A summary of Wallimann's results are shown in Table 4.1. Wallimann's predicted change in R on excitation from the ground to excited state was determined using his reported spectroscopic parameters in a Franck-Condon simulation.

Table 4.1. Spectroscopic constants for Au-Kr reported by Wallimann.[1] Details in text.

	$X^2\Sigma_{1/2}^+$	$D^2\Pi_{1/2}$	$D^2\Pi_{3/2}$
ω_e / cm^{-1}	23.8 ± 0.1[a]	140.2 ± 2.7	146.6 ± 2.7
$\omega_e x_e$ / cm^{-1}	0.787 ± 0.049[a]	1.922 ± 0.027	1.165 ± 0.074
T_0 / cm^{-1}	-	(35035 ± 41)[b]	(36808 ± 325)[b]
D_e / cm^{-1}	180 ± 10[b]	2557 ±41	4612 ± 325
D_0 / cm^{-1}	168 ± 10[b]	2487 ± 41	4539 ± 325
$R_e' - R_e''$ / Å [c]	-	-1.08 ± 0.05	-1.03 ± 0.05

[a] From analysis of hot bands, and using the average ground state dissociation energy derived from the excited states.

[b] Not observed, extrapolated from Birge-Sponer analysis.

[c] From Franck-Condon factors, and using estimate of $R_e \approx 3.83$Å for $X^2\Sigma_{1/2}^+$ state.

The work presented herein reports new spectra, in addition to a re-analysis of the spectra reported by Wallimann, re-evaluating the absolute vibrational numbering, and therefore deriving a revised set of spectroscopic constants. Calculated potential energy curves in addition to Franck-Condon simulations also shed further light on the spectroscopy in this energetic region.

4.2 Experimental procedure

The experimental procedure used in this experiment is described in detail in Chapter 2. For the formation of Au-Kr complexes, the backing gas consisted of 0.05 bar of Kr topped up to 11 bar with Ar. A (1+1) REMPI scheme was employed to investigate the $D^2\Pi_{1/2} \leftarrow X^2\Sigma_{1/2}^+$ transition in which the frequency doubled output of a Sirah dye laser,

employing Coumarin 540A, pumped by the third harmonic of a Surelite III Nd:YAG laser was used for both the excitation and ionization steps. For the $D^2\Pi_{3/2} \leftarrow X^2\Sigma_{1/2}^+$ spectrum recorded in Nottingham a (1+1′) REMPI scheme was employed. The excitation step was achieved using the frequency doubled output of a Sirah dye laser, using Coumarin 480 dye, pumped by the third harmonic of a Surelite III Nd:YAG laser. The second harmonic of the same Nd:YAG laser was used to pump a second Sirah dye laser, employing the dye Rhodamine B. The frequency doubled output of this second dye laser was used for the subsequent ionization step.

In Nottingham attempts were made to enable the recording of the individual isotopomers of Au-Kr, although on the whole unsuccessful, the logic behind them is sensible and therefore worth noting. The idea was to extend the time taken for the ions to reach the detector and hence also increase the time separation between. Initial attempts at achieving a longer TOF of the ions centred on adjusting (lowering) the voltages on the repeller plates in order to reduce the initial repulsion felt by the ions, however, this resulted in a loss of signal sufficient enough that useful spectra could not be obtained. The lengthening (by 0.5 meters to give a 1 meter) of the TOF tube, with subsequent adjustment of the repeller plates, was also attempted but in this case no signal was observed at all. In the end the standard 0.5 meter TOF tube was used with the repeller plates were set in order to maximize the observed total signal, with +800 V on the bottom plate and +680 V on the top plate.

4.3 Results

4.3.1 Overview of Au-Kr spectra

The spectra recorded for the $D^2\Pi_{1/2} \leftarrow X^2\Sigma_{1/2}^+$ transition at Nottingham, in addition to the isotopically-resolved spectra reported in Wallimann's thesis are shown in Figure 4.1. The spectra recorded by Wallimann in Bern were obtained using "soft" conditions where the laser beam had been expanded to alleviate saturation of signal and minimize power broadening.[1] Furthermore, the spectrum recorded at Nottingham is not fully mass resolved and therefore each observed peak has contributions from a number of isotopomers and therefore appears somewhat broader than those obtained at Bern. Comparison of the line positions indicate that the Nottingham spectrum is dominated, as expected, by the most prevalent isotopomer, ^{197}Au-^{84}Kr. The vibrational spacings of the Nottingham and Bern spectra agree, although the absolute calibration is observed to be slightly different. Both spectra are very similar, with an additional feature being observed to higher energy in the Nottingham spectrum. As in Au-Ar, the $D^2\Pi_{1/2}$ state spectrum is red shifted from the atomic origin suggesting that the observed state is more strongly bound than that of the ground state. The features exhibit consistent vibrational spacings and band profile; an initial glance at the Franck-Condon profile suggests that the electronic origin is not observed. The line position of the features of all the spectra for the $D^2\Pi_{1/2} \leftarrow X^2\Sigma_{1/2}^+$ transition are reported in Table 4.2

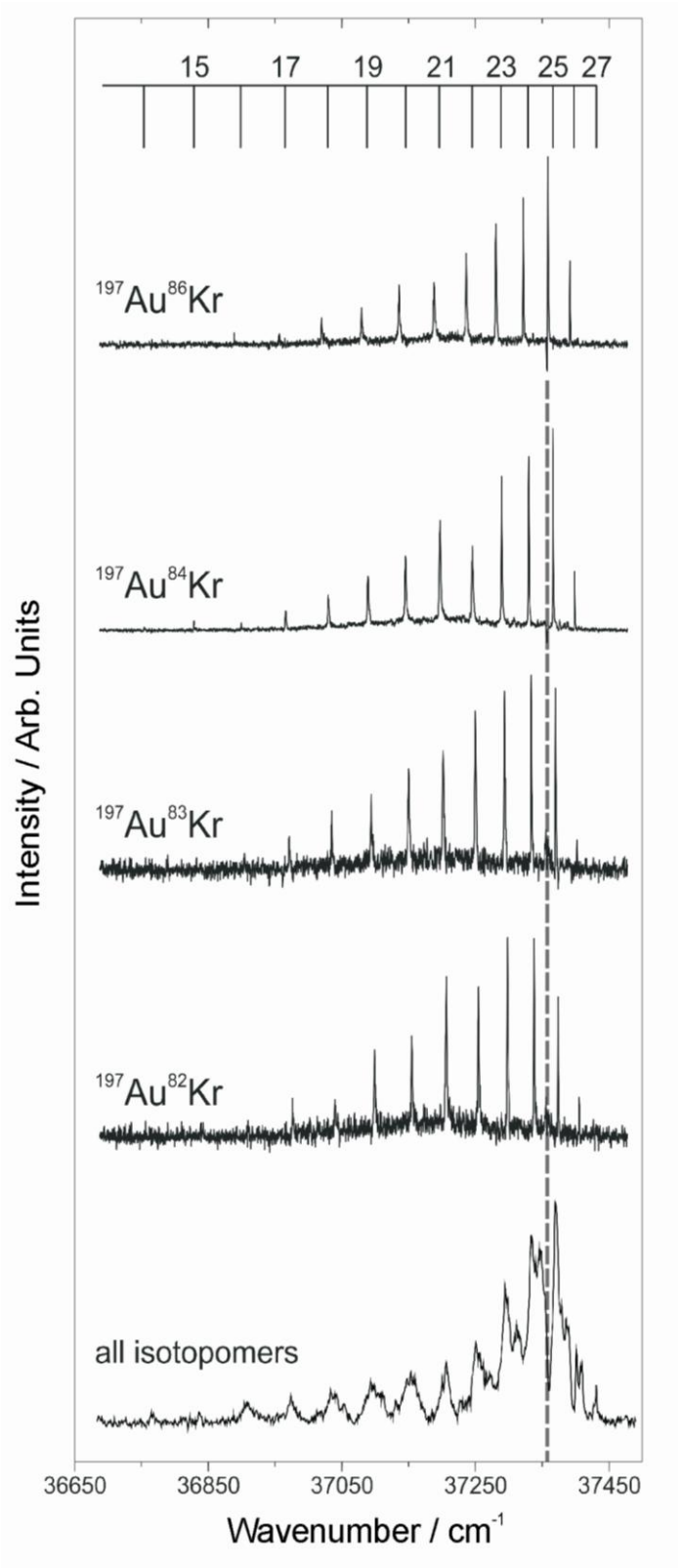

Figure 4.1. Spectra recorded for the $D^2\Pi_{1/2} \leftarrow X^2\Sigma_{1/2}^+$ Au-Kr transition. The top four isotopically resolved traces were recorded at Bern,[1] whilst the bottom trace showing all the isotopomers was recorded in Nottingham. The absolute vibrational numbering is given; the determination of which is described in the section 4.2.2. The dashed line represents the Au $^2P_{1/2} \leftarrow {}^2S_{1/2}$ transition.

Table 4.2. Assignment of features observed for the $D^2\Pi_{1/2} \leftarrow X^2\Sigma_{1/2}^+$ transition. The positions for "all isotopomers" was determined at Nottingham, whilst the isotopically resolved complexes were recorded at Bern.[1]

	Line positions (cm^{-1})					
		Isotopically resolved				
$v' \leftarrow v''=0$	All isotopomers	Au-^{86}Kr	Au-^{84}Kr	Au-^{83}Kr	Au-^{82}Kr	Au-^{81}Kr
14	36753.2	-	36755.6	-	-	-
15	36825.5	36820.1	36830.1	36835.2	-	-
16	36898.7	36890.3	36900.5	36905.7	36911.5	-
17	36965.5	36958.0	36967.3	36972.7	36978.0	36988.3
18	37025.8	37021.3	37031.1	37036.1	37041.4	37205.0
19	37086.9	37081.0	37090.7	37095.7	37100.9	37100.9
20	37148.0	37137.4	37146.7	37151.8	37156.4	37166.5
21	37201.9	37189.4	37198.7	37203.3	37208.3	37217.6
22	37246.9	37237.9	37246.8	37251.4	37255.8	37265.2
23	37291.1	37282.3	37290.9	37295.3	37299.7	37308.7
24	37330.6	37323.1	37331.3	37335.2	37339.4	37347.9
25	37367.5	37360.1	37367.6	37371.3	37375.0	37383.1
26	37399.7	37393.0	37400.0	37403.6	37407.1	37414.1
27	37430.3	-	-	-	-	-

The spectra obtained for the $D^2\Pi_{3/2} \leftarrow X^2\Sigma_{1/2}^+$ transition are shown in Figure 4.2. The top trace is the spectrum recorded using a (1+1) REMPI scheme in Bern, whilst the bottom trace is recorded using a (1+1′) REMPI scheme in Nottingham. As with the $D^2\Pi_{1/2} \leftarrow X^2\Sigma_{1/2}^+$ transition, the features observed in the Nottingham spectrum contains contributions from a number of isotopomers whilst the Bern spectrum is isotopically mass resolved and therefore the features appear narrower. Comparison of the line positions suggests that the Nottingham spectrum is dominated by the ^{197}Au-^{84}Kr spectrum. Again the vibrational spacings of the two spectra are in close agreement, with a slight discrepancy in the absolute calibration. The features exhibit consistent vibrational spacings and rotational profiles throughout the spectrum. The spectrum is redshifted from the atomic transition whilst the appearance of the Franck-Condon profile

suggests that the atomic origin is not observed. The most striking observation of the $D^2\Pi_{3/2}$ spectrum is that it is considerably narrower than that observed for the $D^2\Pi_{1/2} \leftarrow X^2\Sigma_{1/2}^+$ transition. This is contrary to expectations from previous work on the Au-Ar complex (Chapter 3) that suggested that the $D^2\Pi_{3/2}$ is likely to be more strongly bound than the corresponding $D^2\Pi_{1/2}$ state. The peak positions for the spectra displayed in Figure 4.2 are reported in Table 4.3.

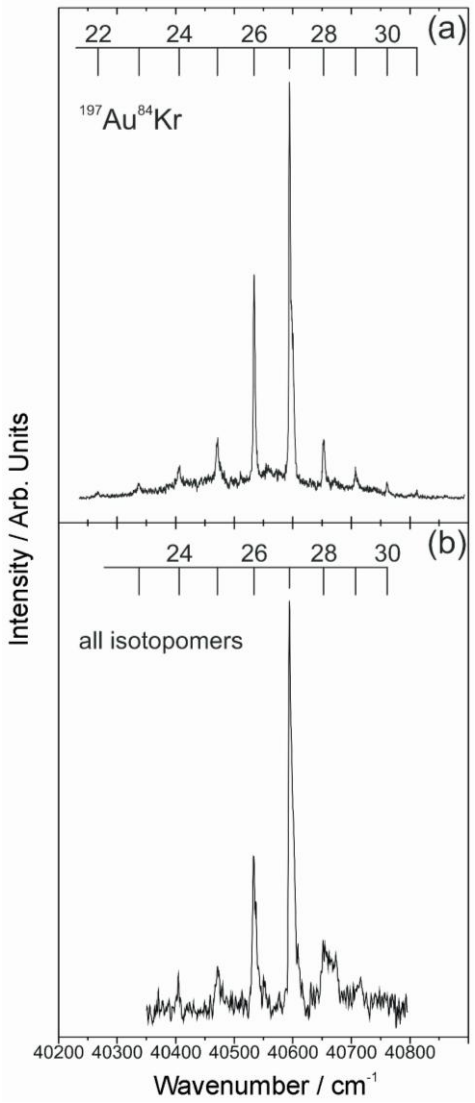

Figure 4.2. Au-Kr $D^2\Pi_{3/2} \leftarrow X^2\Sigma_{1/2}^+$ spectra. The top trace is spectrum recorded using a (1+1) REMPI scheme in Bern,[1] whilst bottom trace is recorded using (1+1′) REMPI scheme in Nottingham. Absolute vibrational numbering is determined using isotopic analysis of features reported in Table 4.3.

Table 4.3. Assignment of features observed for the $D^2\Pi_{3/2} \leftarrow X^2\Sigma_{1/2}^+$ transition. The positions for "all isotopomers" was determined at Nottingham, whilst the isotopically resolved complexes were recorded at Bern.[1]

	Line positions (cm^{-1})					
		Isotopically resolved				
$v' \leftarrow v''=0$	All isotopes	Au-^{86}Kr	Au-^{84}Kr	Au-^{83}Kr	Au-^{82}Kr	Au-^{81}Kr
22	-		40267.2	-	-	-
23	-	40323.2	40337.5	40348.0	-	-
24	40409.9	40391.9	40406.1	40412.5	40420.0	-
25	40476.8	40456.9	40471.4	40477.4	40483.5	40501.9
26	40538.4	40520.4	40533.7	40540.8	40548.3	40562.4
27	40599.7	40580.7	40594.3	40601.0	40608.4	40622.2
28	40657.2	40638.6	40652.6	40659.5	40666.2	40681.4
29	40708.7	40694.7	40707.3	40715.8	40721.9	40738.9
30	-	40747.4	40761.1	40768.5	40774.5	40789.8
31	-	-	40811.9	40818.5	-	-

4.3.2 Isotopic analysis: Determination of absolute vibrational numbering

For the determination of spectroscopic constants from observed vibrational features it is important that the absolute vibrational numbering is known. This is not always as simple as it sounds, as often, as is the case for the spectra reported in this work, the first observed peak is not that of the electronic origin i.e. $v'=0 \leftarrow v''=0$. The absence of the electronic origin in most case is owing to unfavourable Franck-Condon factors for the transition meaning that the transition is too weak to be observed.[3] However, if spectra are recorded for two or more isotopomers, it is possible to make use of isotopic shifts to assign the vibrational numbering. If it is assumed that each isotopic progression fits a Morse potential by plotting the vibrational spacings as a Birge-Sponer plot (see section 3.3.2) an absolute value of $\omega_e' x_e'$ can be determined for each isotopomer. By assuming an initial trial

value ξ for the first observed vibrational quantum number, a value of ω_e' may be determined heuristically for each value of ξ. Within the approximation of the Morse equation, it is then possible to determine theoretical shifts *via* the equation 4.1[4]

$$\Delta\upsilon = (1 - \rho)\ \omega_e (\upsilon + ½) - (1 - \rho)^2\ \omega_e x_e (\upsilon + ½)^2 \qquad (4.1)$$

where, $\Delta\upsilon$ is defined as the isotopic shift of a vibrational feature between a particular isotopomer and that of, for example, the heaviest. ρ is defined as

$$\rho = \sqrt{\mu / \mu_i} \qquad (4.2)$$

where μ_i is the mass of the heaviest isotopomer and μ is the mass of the other isotopomer of interest. Therefore for each value of ξ, a theoretical curve of $\Delta\upsilon$ vs. $(\upsilon' - \xi)$ may be constructed.[4] A plot of the calculated experimental shifts can then be compared to the theoretical curves and hence the absolute vibrational numbering determined.

In Tables 4.2 and 4.3 the vibrational features observed by Wallimann[1] for five isotopomers are shown. This enabled a number of isotopic shifts to be compared and hence an estimate of the absolute vibrational numbering of the features to be determined. Figure 4.3 shows the re-analysis of Wallimann's reported isotopic shifts in both the $D^2\Pi_{1/2}$ and $D^2\Pi_{3/2}$ states. For consistency, only the vibrational levels observed in the spectra for all the isotopomers have been

considered, hence for both states the fourth peak observed for ^{197}Au-^{84}Kr was the first vibrational level considered.

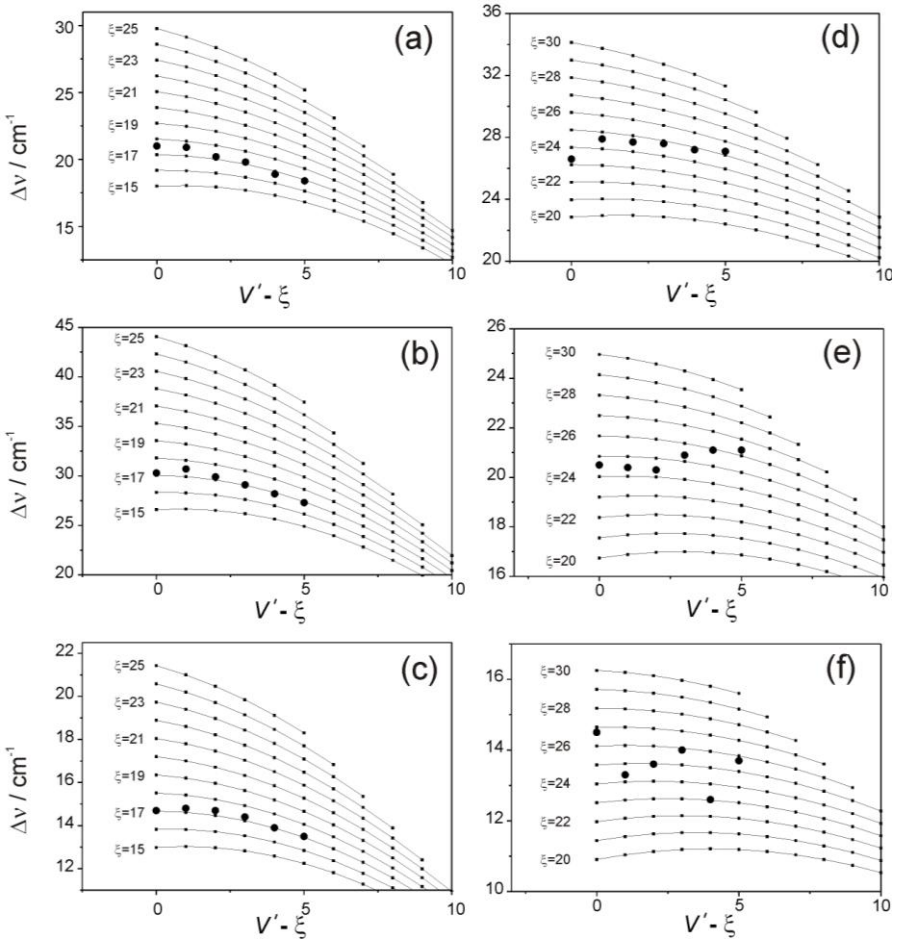

Figure 4.3. Re-analysis of Isotopic shifts reported by Wallimann[1] for the $D^2\Pi_{1/2}$ spectra [(a) – (c)] and $D^2\Pi_{3/2}$ spectra [(d) – (f)]. The isotopomers compared for each of the plots are as follows (a) $Au^{80}Kr$ and $Au^{84}Kr$, (b) $Au^{80}Kr$ and $Au^{86}Kr$, (c) $Au^{83}Kr$ and $Au^{86}Kr$, (d) $Au^{82}Kr$ and $Au^{86}Kr$, (e) $Au^{83}Kr$ and $Au^{86}Kr$, (f) $Au^{84}Kr$ and $Au^{86}Kr$.

From plots (a)-(c) in Figure 4.3 it can be clearly seen that for the $D^2\Pi_{1/2}$ state, the most consistent vibrational numbering is $\xi = 17 \pm 1$. A total of ten analyses were performed, one for each pairing of the isotopomers, all of which were consistent with the three plots presented here, although in some cases there was a greater scattering

of the points. The derived vibrational numbering is shown in Figure 4.1.

The determination of the absolute vibrational numbering in the $D^2\Pi_{3/2}$ state was considerably more challenging as the experimentally observed shifts were markedly more scattered, as seen in the three "best" plots presented in Figure 4.3. However, the points did appear in all cases to be scattered around $\xi = 24$ and so this is given as an estimate for the vibrational numbering in the $D^2\Pi_{3/2}$ state with a possible error of ±2. The derived vibrational numbering is presented in Figure 4.2.

It should be noted that this re-analysis of Wallimann's reported spectra has yielded an absolute vibrational numbering different to that obtained by Wallimann. For the $D^2\Pi_{1/2}$ state the vibrational numbering was 2 quanta lower than that previously reported whilst for the $D^2\Pi_{3/2}$ state the vibrational numbering was predicted to be 10 quanta lower. Investigations into the difference between the two sets of numbering suggest that there was a systematic error in the previous analysis which appears to be a result of $(1 - \rho)$ term not being squared.

4.4 Calculation on Au-Kr complexes

Calculations on the $X^2\Sigma_{1/2}^+$ ground state and the molecular states arising from the Au(^2D_J) + Kr($^1S_0$) and Au(^2P_J) + Kr($^1S_0$) asymptotes, similar to those for Au-Ar, described in detail in Chapter 3, were

performed for Au-Kr by other members of the research group. Calculations were again performed by using MOLPRO.[5]

4.4.1 Au-Kr $X^2\Sigma_{1/2}^+$ state

A potential energy curve for the $X^2\Sigma_{1/2}^+$ state was constructed using single point RCCSD(T) calculations employing the relativistic effective core potentials, ECP60MDF and ECP10MDF for Au and Kr respectively. To these ECPs the *d*-aVXZ-PP (X = Q, 5) basis sets were added. These RCCSD(T) calculations were performed using the frozen core approximation in which only the 4*s* and 4*p* electrons of Kr and 5*d* and 6*s* electrons in Au were correlated. Each point was corrected for basis set superposition error using the full counterpoise correction,[6] and then extrapolated to the basis limit using the two point extrapolation procedure of Helgaker and co-workers.[7,8] The potential energy curves were used as input for the LEVEL program[9] as described for Au-Ar. The ^{197}Au and ^{84}Kr isotopes were used for all calculations; the results of these analyses are shown in Table 4.4. In addition a single point energy was calculated at the RCCSD(T)/*d*-aV5Z level R_e using the *d*-apwCV5Z basis set at the RCCSD(T) level where the inner valence Au electrons were included in the correlation treatment to investigate the effect of core-correlation.[4] The 5*s* and 5*p* orbitals of Au overlap with the 3*d* orbitals of Kr so these also need to be included in the correlation treatment; to describe the correlation of these electrons tight functions were added.

Table 4.4. Calculated spectroscopic constants for ^{197}Au-^{84}Kr $X^2\Sigma_{1/2}^+$

Basis Set	R_e/ Å	D_0'' (D_e'')/ cm^{-1}	ω_e''/ cm^{-1}	$\omega_e''x_e''$/ cm^{-1}
d-aVQZ	3.72	234.2 (244.9)	21.6	4.68
d-aV5Z	3.68	252.5 (263.7)	22.6	4.73
d-apwCV5Z	-	(278.7)[a]	-	-
d-aV∞Z	3.64	273.0 (284.8)	23.7	4.75
d-aCV∞Z	-	288(300)[b]	-	-

[a] calculated at the *d*-aCV5Z equilibrium separation.

[b] estimated from the change in D_e between *d*-aV5Z and *d*-aCV5Z.

4.4.2 Au-Kr excited states

The calculations on the excited states of Au-Kr were carried out in a similar manner to those on Au-Ar described in detail in Chapter 3. Initially, single point, single reference RCCSD(T) calculations employing *d*-aug-cc-pVDZ-PP basis sets, were performed to determine where the states arising from the Au(^2D) + Kr(^1S) asymptote cross the higher lying $^2\Pi$ and $^2\Sigma$ states arising from the Au(^2P) + Kr(^1S) asymptote. The calculated potential curves can be seen in Figure 4.4.

Further CASSCF + MRCI + Q calculations on the $D^2\Pi$ and $E^2\Sigma^+$ states employing the aug-cc-pVQZ basis sets described previously were performed. As with Au-Ar the CASSCF + MRCI + Q energies of the two $^2\Pi$ states and the $E^2\Sigma^+$ state were used as the unperturbed energies in state-averaged CASSCF spin-orbit calculations, to determine the spin orbit coupling at each *R*. The results of these calculations are shown in Figure 4.5.

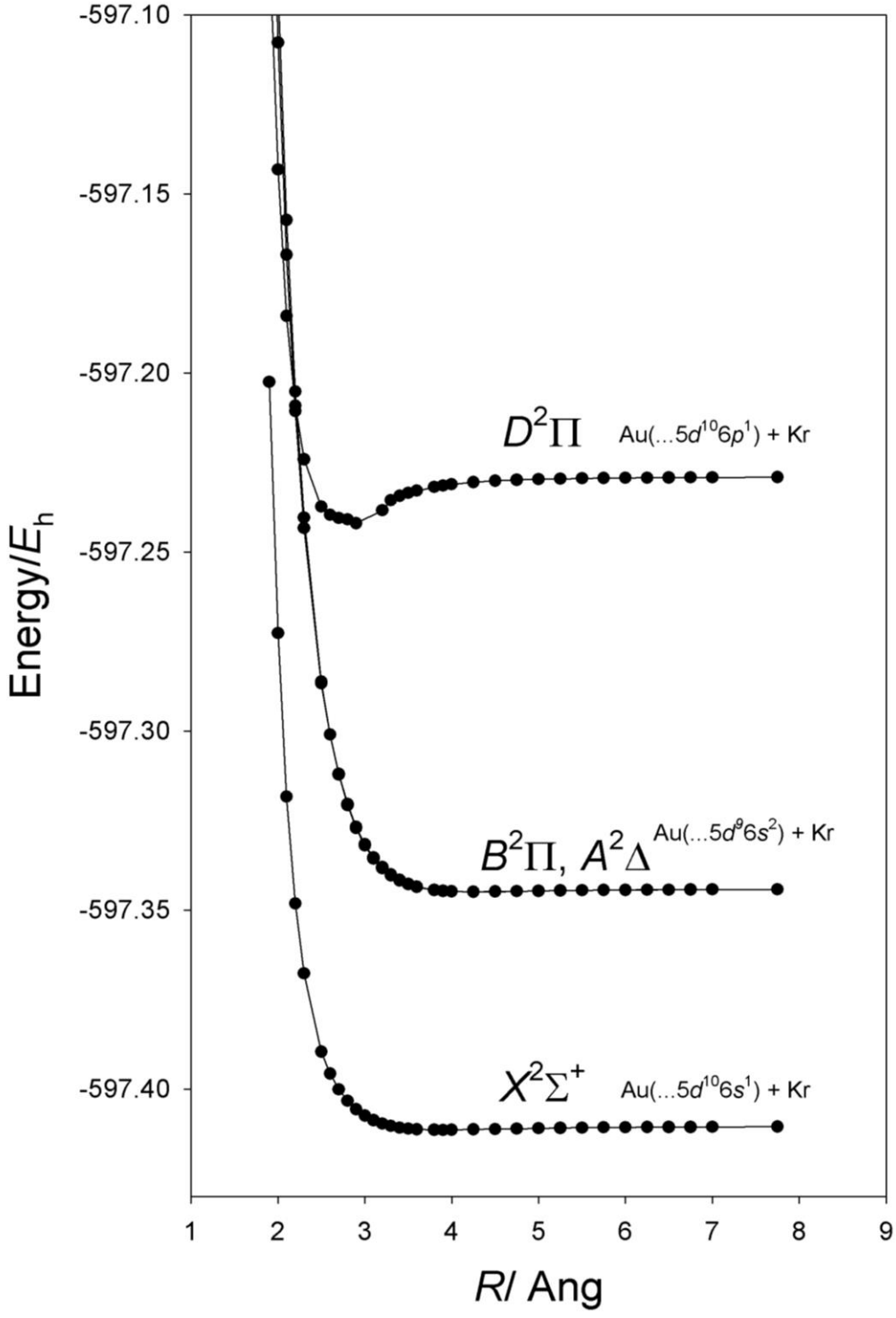

Figure 4.4. Calculated RCCSD(T) potential energy curves for Au–Kr in the absence of spin-orbit interaction. Note that the $A^2\Delta$ state lies slightly lower in energy than the $B^2\Pi$ state (but this is indiscernible on this scale), and that the $C^2\Sigma^+$ state was omitted from the calculations, but is expected to lie slightly above the $B^2\Pi$ state. The $E^2\Sigma^+$ state was also omitted, but lies above the $D^2\Pi$ state.

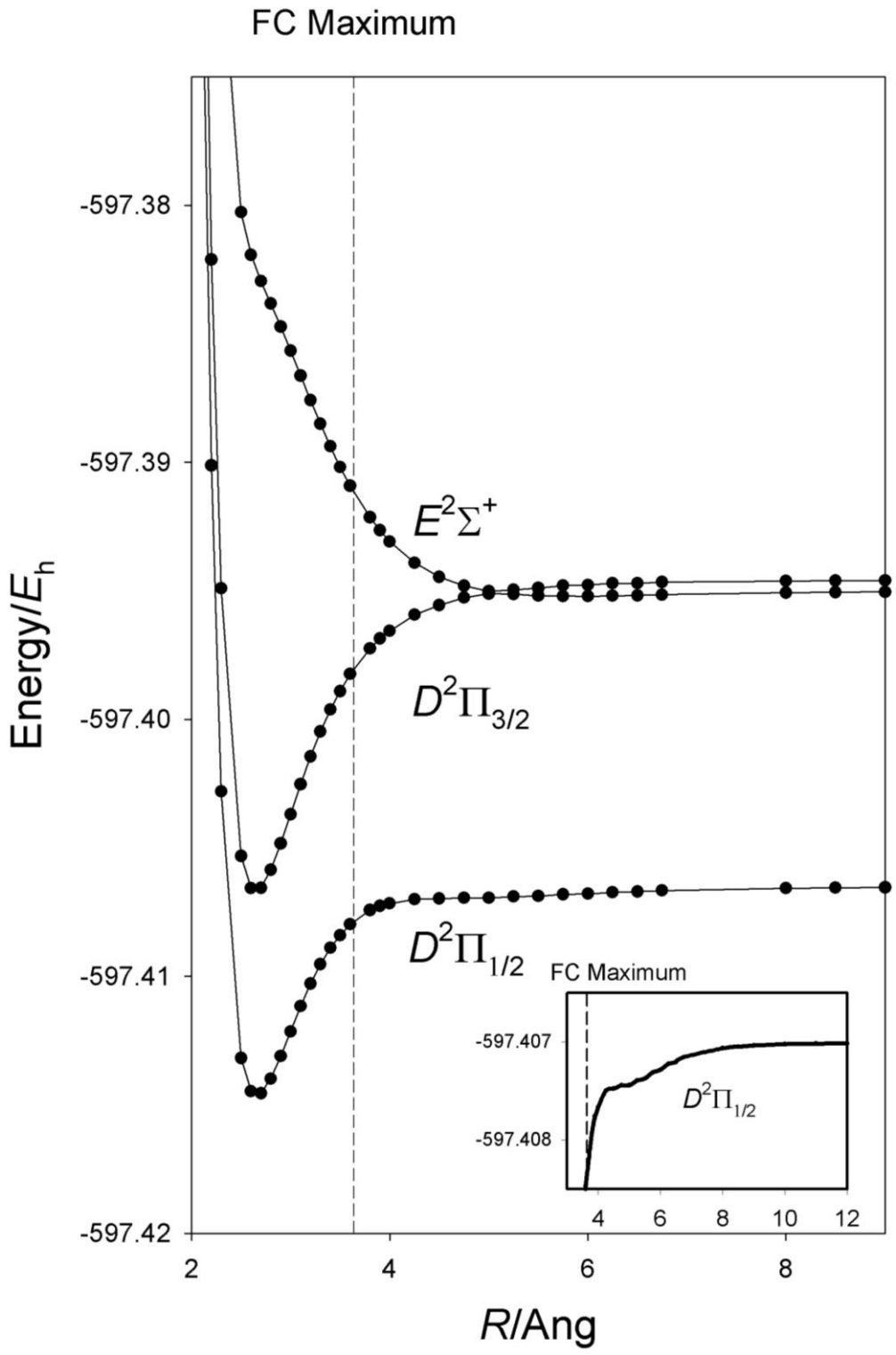

Figure 4.5. CASSCF + MRCI + Q calculations on the $D^2\Pi_\Omega$ and $E^2\Sigma_{1/2}{}^+$ states including spin-orbit coupling. The slight kink in the *E* state potential is due to the mixing with the $D^2\Pi_{1/2}$ state. INSET: expanded view of the *R* region of the $D^2\Pi_{1/2}$ state showing the very shallow minimum caused by mixing with the $E^2\Sigma_{1/2}{}^+$ state.

4.5 Analysis of results and discussion

4.5.1 Determination of experimental spectroscopic constants for Au-Kr

Employing the determined absolute vibrational numbering from this study, spectroscopic constants have been calculated employing the methods discussed in section 3.3.2. Figure 4.6 shows a Morse analysis in addition to Birge-Sponer and LeRoy-Bernstein extrapolations for the vibrational features observed for the $D^2\Pi_{1/2} \leftarrow X^2\Sigma_{1/2}^+$ transition. The results of these analyses are presented in Table 4.5.

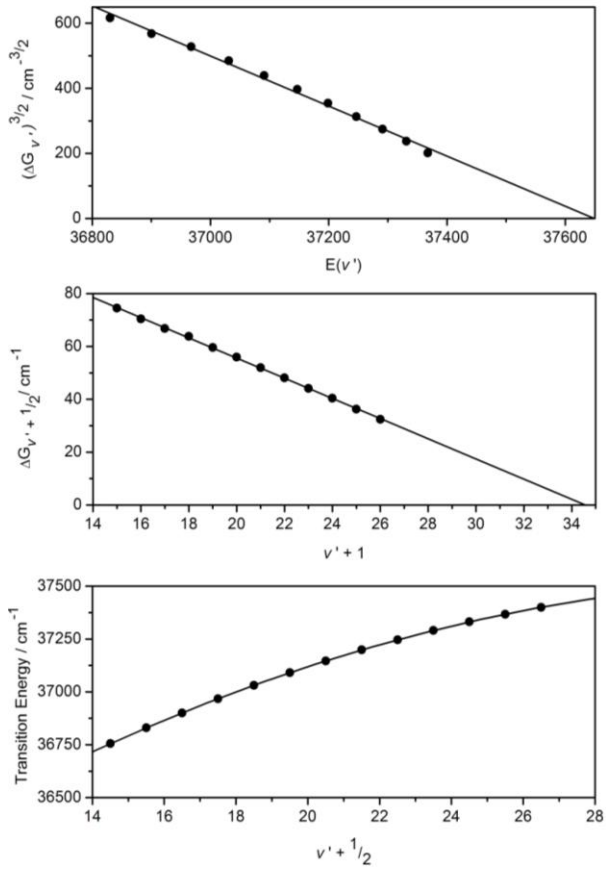

Figure 4.6. Analysis of vibrational features observed for the ^{197}Au-^{84}Kr $D^2\Pi_{1/2} \leftarrow X^2\Sigma_{1/2}^+$ transition. The top plot is that of a LeRoy-Bernstein extrapolation extrapolated to show D_L. The Birge-Sponer plot (middle) is extrapolated to show v' at the dissociation limit. The fitting of the vibrational levels to the Morse approximation is shown in the bottom plot. Results are reported in Table 4.5.

Table 4.5. Spectroscopic constants (cm^{-1}) obtained using vibrational features of $D^2\Pi_{1/2} \leftarrow X^2\Sigma_{1/2}^+$ spectrum of ^{197}Au-^{84}Kr.

Spectroscopic constant	LeRoy-Bernstein extrapolation	Birge-Sponer extrapolation	Morse analysis
D_L	37650.73	37521.74	37459.2
ω_e'	-	132.0	132.1
$\omega_e' x_e'$	-	1.91	1.91
T_0	-	-	35241.30
D_0'	-	2280.74	2218.15
D_0''	291.74	162.748	100.16

A comparison of the results presented in Table 4.5 shows a big discrepancy in the $D^2\Pi_{1/2}$ state D_L values obtained between the different methods. As would be expected, the Birge-Sponer extrapolation and Morse analysis are in a reasonable agreement; however the LeRoy-Bernstein value is considerably higher. Using these D_L values with the Au $^2P_{1/2} \leftarrow {}^2S_{1/2}$ atomic transition an estimate of ground state dissociation value can be obtained from each of these methods, shown in Table 4.5. As can be seen the D_0'' value, estimated using the LeRoy-Bernstein D_L value, is in excellent agreement with that obtained from *ab initio* calculations, whilst those obtained from the Morse and Birge-Sponer D_L values are considerably lower. The vibrational numbering for the observed features seen in Figure 4.1, on which the three analyses are based, suggests that the features observed will be high in the potential well. If this is the case, and the observed features are close to the dissociation limit, it is likely that the values of D_L and D_0'' derived from the LeRoy-Bernstein extrapolation are more reliable, owing to the Morse potential becoming less reliable as long range forces become increasingly dominant. It can therefore also be expected that the Morse and Birge-Sponer methods underestimate the dissociation energy of the $D^2\Pi_{1/2}$ state.

Figure 4.7 shows a Morse analysis in addition to a Birge-Sponer and LeRoy-Bernstein extrapolation for the vibrational features observed for the $D^2\Pi_{3/2} \leftarrow X^2\Sigma_{1/2}^+$ transition. The results of these analyses are presented in Table 4.6.

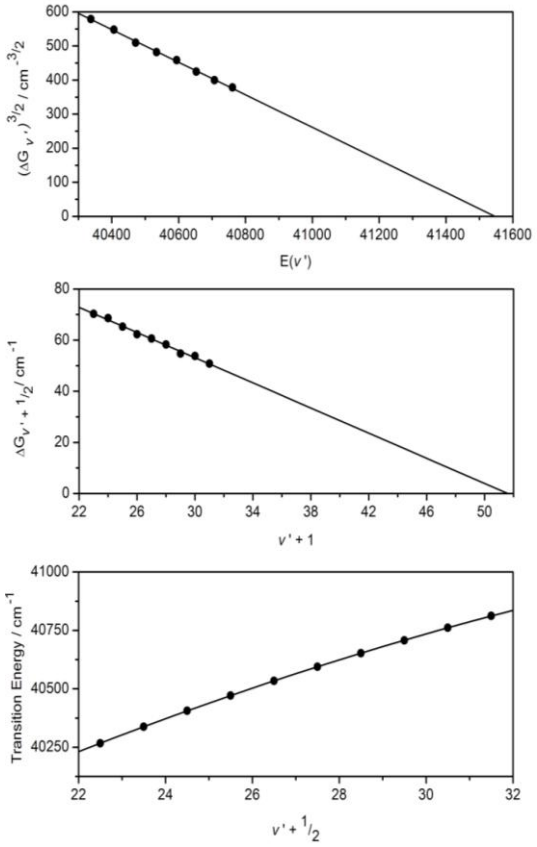

Figure 4.7. Analysis of vibrational features observed for the ^{197}Au-^{84}Kr $D^2\Pi_{3/2} \leftarrow X^2\Sigma_{1/2}^+$ transition. Top plot: LeRoy-Bernstein plot extrapolated to show D_L. Middle: Birge-Sponer plot extrapolated to show v' at D_L. Bottom: Vibrational levels are fitted to Morse approximation. Results are reported in Table 4.6.

Table 4.6. Spectroscopic constants (cm^{-1}) obtained using vibrational features of $D^2\Pi_{3/2} \leftarrow X^2\Sigma_{1/2}^+$ spectrum of ^{197}Au-^{84}Kr.

Spectroscopic constant	LeRoy-Bernstein extrapolation	Birge-Sponer extrapolation	Morse analysis
D_L	41542	41308.16	41242.86
ω_e'	-	126.9	127.1
$\omega_e' x_e'$	-	1.23	1.23
T_0	-	-	38099.67
D_0'	-	3275.16	3209.86
D_0''	367.87	133.54	68.25

Comparison of the results shown in Table 4.6 again display a massive difference between the D_L values derived using the Morse and Birge-Sponer analysis and those obtained using the LeRoy-Bernstein method. However, deriving the ground state dissociation energies as before, it can be seen that there is also a considerable difference between the D_0'' value obtained when employing the LeRoy-Bernstein D_L value *via* the $D^2\Pi_{3/2}$ state and that obtained *via* $D^2\Pi_{1/2}$ state. Although only a qualitative picture can be obtained, examination of the Birge-Sponer analysis suggests that the value of v' at the dissociation limit is ~34 and ~51 for the $D^2\Pi_{1/2}$ and $D^2\Pi_{3/2}$ states respectively. This indicates that it is likely that the vibrational levels observed for the $D^2\Pi_{1/2}$ state were considerably closer to the dissociation limit than those observed for $D^2\Pi_{3/2}$ state. It can therefore be expected that the most accurate value for D_L and hence D_0'' will be that obtained *via* the LeRoy-Bernstein analysis of the $D^2\Pi_{1/2}$ state. This result is also in reasonable agreement with very recent studies[10] using VMI which predicts a ground state dissociation energy of the Au-Kr complex to be 240±19 cm^{-1}. Comparison of the current results to those reported in Wallimann's thesis[1] shows a large discrepancy in most cases; however this is to be expected owing to the difference observed in the absolute vibrational numbering from which most of the parameters are calculated. As it is felt the present numbering scheme is more reliable it is expected that this would also be the case for the calculated spectroscopic constants.

In Au-Ar there was an obvious discontinuity in the observed vibrational progression of the $D^2\Pi_{1/2}$ state, owing to a perturbation in

the attractive limb of its potential; a result of spin-orbit interactions between the $D^2\Pi_{1/2}$ and the $E^2\Sigma_{1/2}{}^+$states. From the results of the CASSCF + MRCI + Q calculations shown in Figure 4.5 it can be seen that there is a similar perturbation in the Au-Kr $D^2\Pi_{1/2}$ state potential. However, apart from possibly a small change in the band profile of the peaks (with the higher energy peaks being slightly narrower) there is little evidence of this perturbation in the Au-Kr $D^2\Pi_{1/2}$ state spectrum. By using the calculated $X^2\Sigma_{1/2}{}^+$ state R_e value and the results of the CASSCF + MRCI + Q calculations it is possible to estimate the Franck-Condon maximum as shown in Figure 4.5. It should be noted that ideally in this situation R_0 and not R_e would be used to determine the Franck-Condon maximum. However, as there is expected to be very little, if any, difference between these two values in this complex, it is felt that R_e, which is directly determined in calculations, is adequate in this situation. As can be seen in Figure 4.5 the predicted perturbation of the $D^2\Pi_{1/2}$ potential is above the Franck-Condon maximum and therefore an observed discontinuity in vibrational spacings and band profiles as reported for Au-Ar is not expected, which is in agreement with experimental observations. The predicted position of the Franck-Condon maximum is also in agreement with deductions made from experimental results that the observed vibrational levels are closer to the dissociation limit for the $D^2\Pi_{1/2}$ state than those observed for $D^2\Pi_{3/2}$ state.

Analysis of the hot bands observed in the spectra yields an estimate of 22.8 ±1.6 cm^{-1} for the 0-1 vibrational spacing in the $X^2\Sigma_{1/2}{}^+$ state. This

value is in excellent agreement the calculated value of $\omega_e'' - 2\omega_e''x_e''$ = 22.8 cm^{-1}.

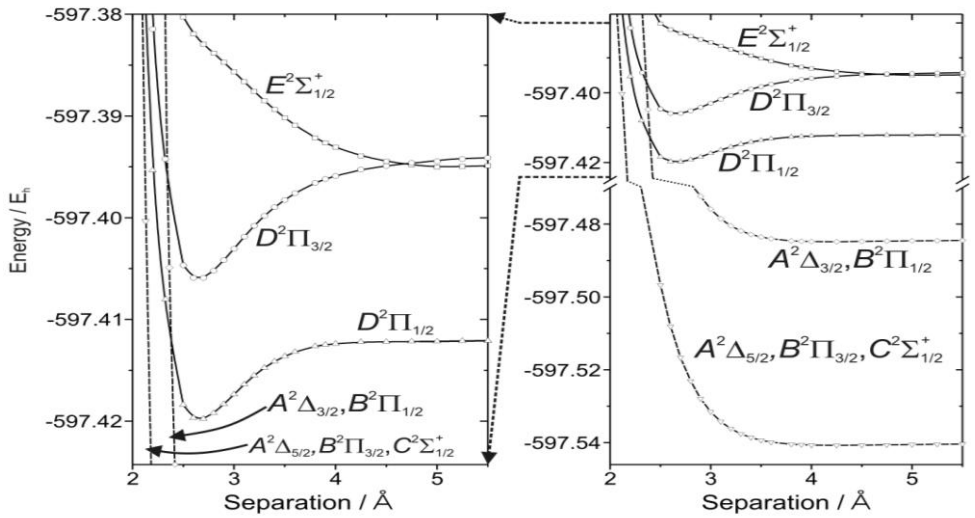

Figure 4.8. Schematic diagram based on the RCCSD(T) and CASSCF + MRCI + Q calculations, showing the spin-orbit curves relevant to the observed spectral region. Right-hand side: Overview. Left-hand side: Expanded view.

As mentioned above, the $D^2\Pi_{3/2}$ state spectrum is significantly narrower than that of the $D^2\Pi_{1/2}$ state spectrum. Considering the relative well depths of the two $^2\Pi$ states and the position of Franck-Condon maximum, this suggests that there must be some mechanism through which the transition to the $D^2\Pi_{3/2}$ state is losing intensity. As can be seen in Figure 4.4 the states arising from the Au(^2D) + Kr(^1S) asymptote cross very close the bound region of those arsing form the Au(^2P) + Kr(^1S) asymptote. Figure 4.8 is a schematic based on the RCCSD(T) and CASSCF + MRCI + Q calculation described in section 4.3.1 and 4.3.2, in which the spin orbit interactions in the states arising from the Au(^2D) + Kr(^1S) asymptote have been approximated to obtain an overall picture of the crossings occurring in the Au ($^2P \leftarrow {}^2S$) energetic region. The states arising from the Au(^2D) + Kr(^1S) asymptote

can be seen to split in to two groups; an upper pair comprising the $A^2\Delta_{3/2}$ and $B^2\Pi_{1/2}$ states and a lower trio comprising the $A^2\Delta_{5/2}$, $B^2\Pi_{3/2}$ and $C^2\Sigma_{1/2}^+$ states. Of these two groups it is the upper pair that is of relevance in this discussion. As the $B^2\Pi_{1/2}$ state approaches the $D^2\Pi_{1/2}$ state it undergoes an avoided crossing induced by configuration interaction, however as can see in Figure 4.8 this crossing is likely to occur above the $D^2\Pi_{1/2}$ dissociation limit and thus will have little effect on the overall shape of the two curves except in the immediate vicinity of the avoided crossing. The $A^2\Delta_{3/2}$ state crosses close to the bound region of the $D^2\Pi_{3/2}$ state potential; this would allow vibrational levels in the $D^2\Pi_{3/2}$ state to predissociate into the $A^2\Delta_{3/2}$ state continuum. As the two curves become increasingly close to one another in respect to R as they go to higher energy (until the eventual crossing point) it is expected that the efficiency of the predissociation mechanism will increase, resulting in the higher vibrational levels not being observed.

4.5.2 Franck-Condon Simulations

Franck-Condon simulations of the Au-Kr $D^2\Pi_{1/2}$ and $D^2\Pi_{3/2}$ state spectra were performed. In the simulations, the spectroscopic parameters determined at the RCCSD(T)/*d*-aV∞Z level of theory (reported in Table 4.4) were used for the $X^2\Sigma_{1/2}^+$ ground state, as these are believed to be the most reliable, whilst the spectroscopic parameters reported in Table 4.5 and Table 4.6 were used for the $D^2\Pi_{1/2}$ and $D^2\Pi_{3/2}$ states, respectively.

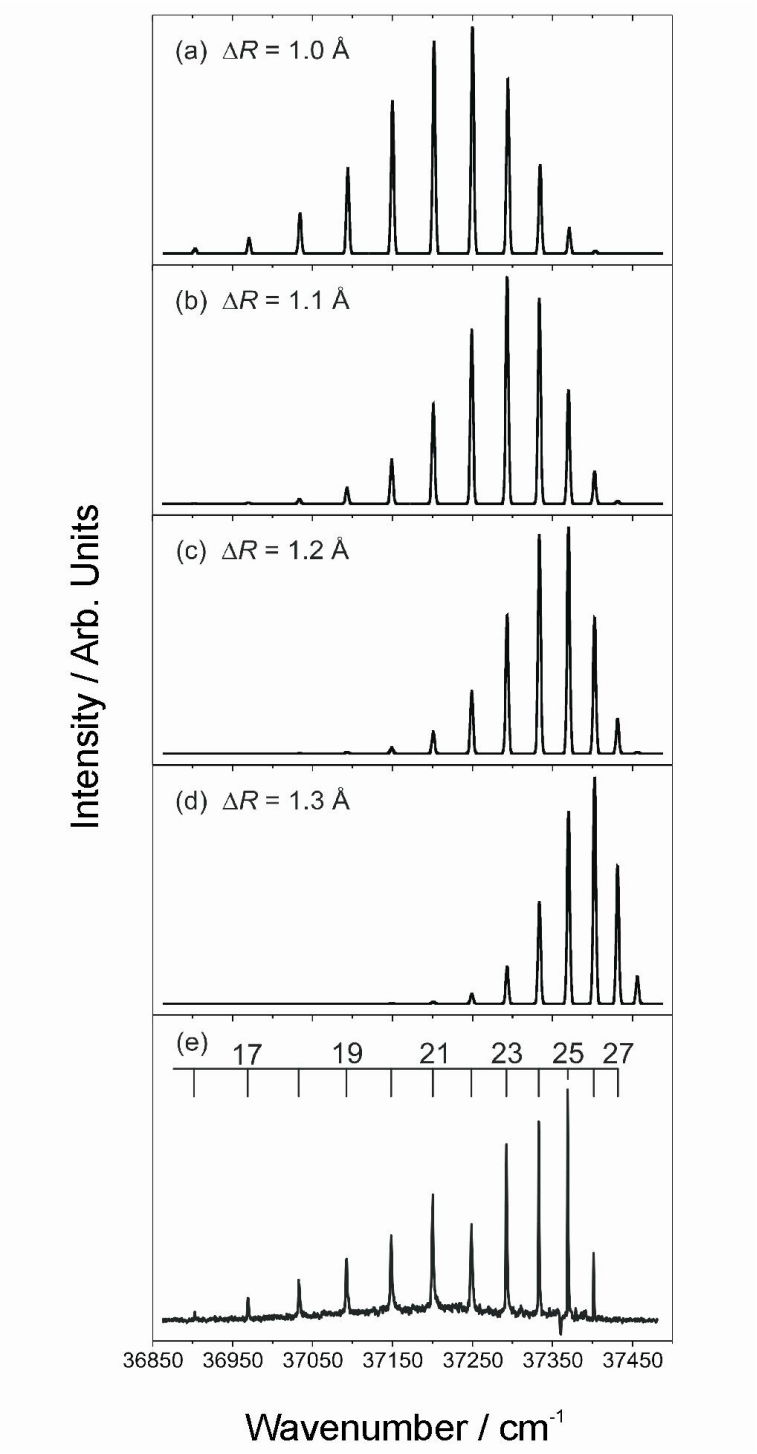

Figure 4.9. The Franck-Condon simulation of the $D^2\Pi_{1/2} \leftarrow X^2\Sigma_{1/2}^+$ transition – see text for details. The simulated spectrum has been scaled so that the most intense feature matches that of the corresponding experimental one (trace e).

Simulations for the $D^2\Pi_{1/2}$ state shown in Figure 4.9 were achieved by varying R_e of the excited state with respects to that of the ground state to obtain the closest fit possible. As can be seen, the overall profile of

the fit is good, with the main discrepancy being to lower energy. This can be attributed in some part to saturation of the most intense features similar to that observed for Au-Ar. The best fit was judged on the appearance of the fit to be in the range of $1.10 \leq \Delta R_e \geq 1.30$Å, hence a conservative estimate for internuclear separation in the $D^2\Pi_{1/2}$ state would be $R_e = 2.45 \pm 0.10$ Å assuming that ΔR_e is negative owing to stronger bonding in the $^2\Pi_\Omega$ states than in the $X^2\Sigma_{1/2}^+$ state. These results are in good agreement with those obtained *via* CASSCF + MRCI + Q calculations which give $\Delta R_e = 1.24$ Å and R_e of the $D^2\Pi_{1/2}$ state as 2.66 Å which, although slightly out of the derived range from the simulations, is in line with the limited treatment of dynamic correlation in those calculations.

The CASSCF + MRCI + Q calculations suggest that the two $^2\Pi_\Omega$ states have almost identical R_e values (within 0.01Å), therefore using the value of R_e derived for the $D^2\Pi_{1/2}$ state and the spectroscopic parameters reported for the $D^2\Pi_{3/2}$ state a simulated spectrum for the $D^2\Pi_{3/2}$ state was produced. The simulated spectrum shown in Figure 4.10 can be seen to extend considerably further to the blue than the experimentally observed spectrum, in line with expectations from the hypothesis that the higher vibrational levels of this potential predissociate into the $A^2\Delta_{3/2}$ state continuum. A comparison of the first few simulated features, normalized by the matching of the v'=27 simulated peak intensity to that of the most intense experimentally observed peak, shows that there is an excellent match in both intensity and band profile to those obtained experimentally. This analysis, in conjunction with the results from the calculations, is

strong evidence for the predissociation of higher v' levels in the $D^2\Pi_{3/2}$ state affecting the appearance of the spectrum; likely through predissociation into the $A^2\Delta_{3/2}$ state continuum.

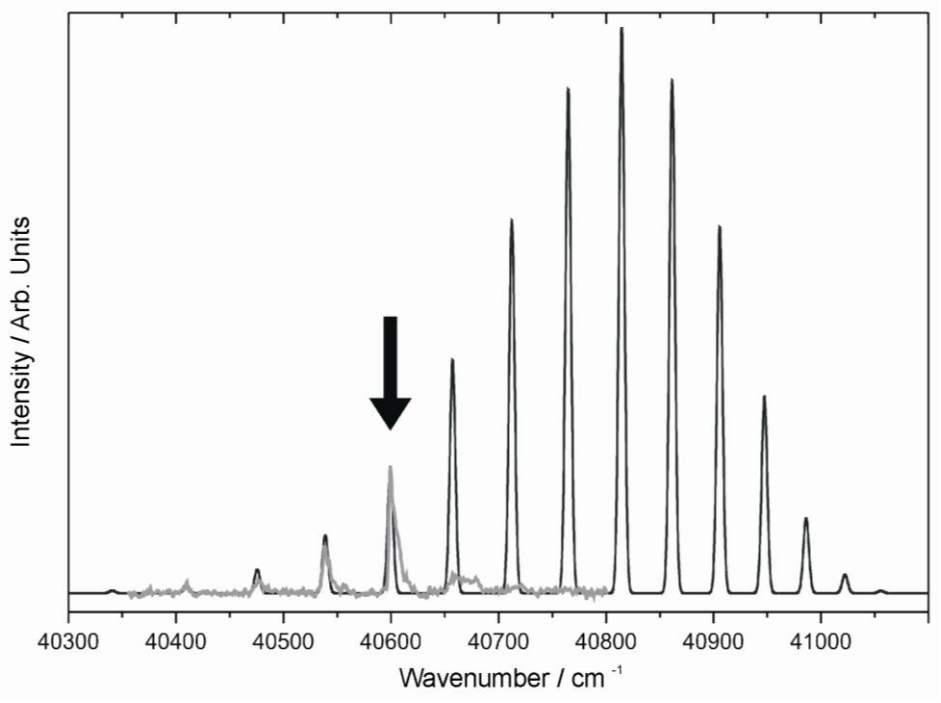

Figure 4.10. Franck-Condon simulation of the $D^2\Pi_{3/2} \leftarrow X^2\Sigma_{1/2}^+$ transition; as can be seen intensity to blue in the experimental spectrum is missing owing to predissociation – see text for details. The simulated spectrum (bold trace) has been scaled so that the intensity of the $v' = 27$ feature (indicated by vertical arrow) matches that of the corresponding experimental one.

4.6 Conclusions

Au-Kr spectra were obtained for the two spin-orbit split $^2\Pi_\Omega$ states in the Au ($^2P \leftarrow {}^2S$) energetic region. A re-analysis of previously recorded spectra[1] yielded a revised absolute vibrational numbering for both observed excited states, which in turn lead to an amendment of the derived spectroscopic constants. A similar perturbation observed in the Au-Ar $D^2\Pi_{1/2}$ state potential was shown to be present in the corresponding Au-Kr state potential; however, no discontinuity was

observed in the latter spectrum as this perturbation was shown to be outside the Franck-Condon window.

The observation of a narrow spectrum for the $D^2\Pi_{3/2}$ state spectrum was rationalized through RCCSD(T) calculations that suggested that the states arising from the Au(^2D) + Kr(^1S) asymptote would cross the bound region of the $^2\Pi_\Omega$ states arising from the Au(^2P) + Kr(^1S) asymptote. It is suggested that the higher vibrational levels of the $D^2\Pi_{3/2}$ state undergo predissociation *via* the $A^2\Delta_{3/2}$ state. This hypothesis is supported by Franck-Condon simulations in which the $D^2\Pi_{1/2}$ spectrum can be satisfactorily simulated whilst the $D^2\Pi_{3/2}$ state simulated spectrum extends considerably further to the blue than that of the experimental spectrum.

References

[1] F. Wallimann, Dissertation *Laserspektroskopie von Metall-Edelgas-Clustern*, Phil.-nat. Fakultät, Universität Bern, 1997.

[2] http://physics.nist.gov/cgi-bin/Compositions/stand_alone.pl?ele=Kr&ascii=html&isotype=some

[3] A. M. Ellis, M. Feher and T. G. Wright, *Electronic and Photoelectron Spectroscopy Fundamentals and Case Studies,* Cambridge University Press, Cambridge, 2005.

[4] R. J. Plowright, A. M. Gardner, M. J. Watkins, T. G. Wright, W. H. Breckenridge, F. Wallimann and S. Leutwyler, *J. Chem. Phys.,* 2008, **129**, 154315.

[5] MOLPRO is a package of *ab initio* programs written by H. J. Werner, P. J. Knowles and others.

[6] S. F. Boys, F. Bernardi, Mol. Phys., 1970, 19, 553.

[7] T. Helgaker, W. Klopper, H. Koch and J. Noga, *J. Chem. Phys.*, 1997, **106**, 9639.

[8] A. Halkier, T. Helgaker, P. Jỳrgensen, W. Klopper, H. Koch, J. Olsen and A. K. Wilson, *Chem. Phy. Lett.*, 1998, **286**, 243.

[9] R. J. LeRoy, LEVEL 7.2 - A computer program for solving the radial Schrödinger equation for bound and quasibound levels, and calculating various expectation values and matrix elements. (University of Waterloo Chemical Physics Research Program Report CP-555R (2000)).

[10] W. S. Hopkins, A. P. Woodham, S. R. Mackenzie, R. J. Plowright and T. G. Wright, *J. Chem. Phys.*, submitted.